Version of Record: https://www.sciencedirect.com/science/article/pii/S0278434320302235
Manuscript_af07fa1871bb13e9876d5858df4b6d18

Wave transmission through living shoreline breakwalls

I.Safak[a,*], C.Angelini[b,c], P.L. Norby [c], N. Dix [d], A. Roddenberry [e],
D. Herbert [b], E. Astrom[b], A.Sheremet[b]

a. Department of Civil Engineering, Faculty of Engineering and Natural Sciences, Istanbul Bilgi University, 34060 Eyupsultan, Istanbul, TURKEY

b. Civil and Coastal Engineering Department, Engineering School of Sustainable Infrastructure & Environment, University of Florida, 365 Weil Hall, P.O. Box 116590, Gainesville, FL 32611, USA

c. Department of Environmental Engineering Sciences, Engineering School of Sustainable Infrastructure & Environment, University of Florida, 365 Weil Hall, P.O. Box 116590, Gainesville, FL 32611, USA

d. Guana Tolomato Matanzas National Estuarine Research Reserve, 505 Guana River Road, Ponte Vedra Beach, FL 32082, USA

e. Florida Fish and Wildlife Conservation Commission, 520 Barracuda Blvd., New Smyrna Beach, FL 32169, USA

Abstract

Living shorelines are being widely implemented to mitigate shoreline erosion and provide ecosystem services, but how they interact with waves remains poorly understood. Wave transmission through living shoreline breakwalls is studied using field observations and theoretical

*Corresponding author. E-mail: ilgar.safak@bilgi.edu.tr

approaches. The following hypotheses are tested: (i) living shoreline breakwalls can act as buffers against waves; (ii) wave transmission through these nature-based solutions is modulated by tides; and (iii) wave transmission through living shoreline breakwalls is similar to the behavior observed in waves through porous breakwaters. Observations were collected in intertidal settings where boat wakes and tides are the major flow components. Nearly 1000 boat wakes were identified in the observations using advanced time-frequency data analysis methods. Wave transmission through the breakwalls composed of tree branches was quantified and modulation of this process by tides was investigated. The two tested breakwall designs provided different behaviors of wave transmission. In the first design with an estimated porosity of 0.7 where the tree branches were bundled, transmission rates were found to vary mostly between 9% and 70% and had an average of 53%. Transmission increased with increasing water depth especially at mid-tide and low-tide where the height of the breakwall relative to depth was between 0.5 and 1. In the second design with an estimated porosity of 0.9 where the tree branches were not bundled, transmission rates exceeded 70% in 84% of the cases, sometimes reaching 100% transmission, and had an average of 83% with much less variability with depth compared to the first design. Wave transmission estimates based on theory of porous media were found to be most sensitive to breakwall porosity and the friction coefficient. Best agreement between the observed and theoretical estimates of wave transmission was found using a turbulent friction coefficient of 2.7, the median value of the most common range given in the literature on waves through porous media. The highest discrepancy between observed and theoretical estimates of wave transmission occurs at shallow depths when the breakwall emerged. In these conditions, the theory overestimates transmitted wave energy, most likely due to significant wave breaking and bottom friction in shallow water. The findings support our hypotheses that well-engineered semi-porous living shorelines act as buffers against human-mediated boat traffic and waves, and their related performance in dissipating wave energy and sustaining coastal ecosystems is modulated by depth. The results can be used as guidelines for design of living shorelines for given wave climate and breakwall properties.

Keywords: wave; boat wakes; porous breakwater; dissipation; living shoreline; erosion; Intra-coastal Waterway

1 Introduction

Natural and anthropogenic stressors on coastal ecosystems are projected to increase due to more extreme and frequent storms caused by climate change and increasing development along the coasts, where population density is already significantly greater than that of inland areas (UNEP , 2007). Excessive wave energy negatively impacts coastal ecosystems by reducing the diversity and mass of vegetation (Keddy, 1982) and obstructing larval recruitment and survival of oyster reefs (Wall et al., 2005). These, in turn, cause more energetic waves, and higher sediment loads at the coast. In estuaries with heavy recreational and commercial boat traffic and limited fetch distance for wind wave generation, boat wakes have the potential to dominate the wave climate instead of more widely acknowledged swell and wind waves. Together with wind-induced currents and tides, these wakes become the major physical control on the ecology, hydrodynamics, and sediment transport in such settings (e.g., Gabel et al., 2017). Boat traffic has a wide variety of direct negative impacts on coastal ecosystems such as damage to larvae and aquatic animals due to ship collision and contact with propellers (including the North Atlantic right whale which is one of the most endangered whales in the world), disturbance to animal communication, movement, nutrition, survival, sheltering and nesting sites (e.g., Walters et al., 2002; Wolter and Arlinghaus, 2003; Kraus et al., 2005; Wall et al., 2005; Kucera et al., 2009; Bulte et al., 2010; Gabel et al., 2017). Some indirect impacts include shoreline and marsh erosion due to their wakes, excessive turbidity, and decreased water quality due to fuel discharge (e.g., Jackivicz and Kuzminski, 1973; Bauer et al., 2002; Parnell et al., 2007).

Due to environmental, economical, and aesthetic concerns, the sustainability of hard structural armoring using rocks or artificial materials to protect coastal communities and infrastructure from excessive wave energy is beginning to be questioned (e.g., Seitz et al., 2006; Dugan et al., 2008). As a result, natural and nature-based solutions are being widely implemented to mitigate shoreline erosion, provide and conserve habitat, and generate other ecosystem services such as carbon sequestration and support of fish and invertebrate biodiversity (e.g., Davis et al., 2015; Bilkovic et al., 2016; Sharma et al., 2016; Davenport et al., 2018; Morris et al., 2018; O'Donnell, 2018; Polk and Eulie, 2018; Smith et al., 2018). However, the suitability of living shorelines needs to be quantitatively assessed in terms of the interaction of the living shorelines with hydrodynamics. Hydrodynamics is the major physical process that controls the flow energy that is transmitted through the living shorelines and reaches the coast, and, therefore, how efficiently these methods support the aforementioned ecosystem services. Evaluating the performance of living shorelines and presenting design guidelines first require collection and analysis of comprehensive data sets on waves, hydrodynamics, and sediment processes. As importantly, the findings need to be evaluated within a theoretical framework for applicability to future studies and widespread implementation. Previous studies on wave transmission through living shorelines estimated transmission qualitatively by comparing wave heights measured onshore and offshore of the breakwalls where the cross-shore variation of depth was significant (Boumans et al., 1997; Ellis et al., 2002). However, transmission needs to be estimated by taking depth variations and resulting wave shoaling into account and by using proper data analysis methods. To the authors' knowledge, this is the first study on wave transmission through living shoreline breakwalls using field observations, proper time-frequency analysis methods, and theoretical approaches.

In this study, the performances of two living shorelines in acting as buffers against waves in intertidal settings are investigated. These living shoreline breakwalls are composed of wooden fence posts and tree branches and varied in their porosity. Comprehensive field observations on generation and propagation of boat wakes are collected and analyzed. Transmission of boat wake energy through breakwalls is quantified. The physical processes and breakwall properties controlling the transmission rates are studied. It is hypothesized in this study that living shoreline breakwalls could act as buffers against waves; their performance would be modulated by tides; and what is known about wave transmission through porous media can be translated to living shoreline breakwalls interacting with boat wakes. Accordingly, results are evaluated with theoretical approaches and findings in the literature on hard engineering structures. The results are presented and discussed in relation to major design aspects such as living shoreline breakwall height and porosity, and water depth variations. These can also be used as first-cut guidelines on the design and performance of these nature-based structures in dissipating wave energy and supporting adjacent coastal ecosystems.

2 Material and Methods

2.1 Field experiments

For this study, a series of field sites were monitored within the Guana Tolomato Matanzas National Estuarine Research Reserve (GTM) and North Peninsula State Park (NP). Both of these sites are located within the Atlantic Intracoastal Waterway (ICW) in Northeast Florida, USA (Figure 1). Florida is the state with the highest number of recreational boat registrations (about one million) in the USA (FLHSMV, 2013). A recent report by the Florida Department of Environmental Protection (FDEP, 2018) showed that out of 825 miles of Florida coastline studied, 52% is critically eroding due to natural and anthropogenic effects. Boat wakes are also specifically identified among the major causes of erosion along the ICW, based on aerial photographs taken since the 1970s (Price , 2005) and field observations of boat wakes, sediment transport, and shoreline change (Safak et al., 2020 and Safak et al., under review).

The field sites in this study are along the ICW close to three inlets that experience very high traffic of recreational boats and vessels year-round (Montes et al., 2016). The GTM field site is in St. Johns County and located west of the Pine Island along the Tolomato River at 30.053^o Latitude North, 81.368^o Longitude West, that is 17 km north of the St. Augustine Inlet and 37 km south of the St. Johns Inlet (Figure 1). The NP field site is located in Ormond Beach in Volusia County, along the Halifax River at 29.399^o Latitude North, 81.095^o Longitude West (Figure 1), and is 58 km south of the St. Augustine Inlet and 41 km north of Ponce Inlet. The shoreline at each site was dominated by smooth cordgrass (*Spartina alterniflora*), with individual black mangrove (*Avicennia germinans*) trees scattered throughout. Typically, expansive reefs of the Eastern oysters (*Crassostrea virginica*) line the lower intertidal margin of salt marshes in the region; however, intensive boat wakes have extirpated these natural reefs from much of the length of the ICW in this region.

Within the scope of this project, a series of porous breakwalls were constructed along the sites at GTM and NP in order to test their performance in dissipating boat wake energy and, therefore, acting as buffers against boat wake induced erosion of the shoreline. The porous nature of the breakwalls is preferred in order to provide the circulation of the river channel water into the ecosystem onshore of the breakwalls and to reduce the likelihood of scour in the vicinity of the breakwalls. The breakwalls built at GTM and NP were approximately 4.3 m long, 0.6 m wide, 0.55 m high and were located approximately 6 m offshore of the vegetation at the shoreline (Figure 2). Each breakwall was built by driving into the ground a set of 14, 2-m-long pressure-treated wooden fence posts. These fence posts were positioned into a rectangle by arranging in two parallel rows of seven posts, with each post spaced 0.6 m in the horizontal from its neighbor. Each fence post was driven into the ground to a depth of at least 0.6 m using augers and large wooden mallets. At GTM, crepe myrtle tree (*Lagerstroemia speciosa*) branches of 5 cm in diameter (d=0.05 m) were bundled into tight packets using 1.6 cm wide embossed polypropylene plastic strapping (McMaster-Carr, Elmhurst, IL, USA) before being placed between the two rows of fence posts and secured in place using plastic-coated multipurpose wire and galvanized staple nails. At NP, eastern cedar branches (*Juniperus virginia*) of 5 cm in diameter were immediately placed between the fence posts, i.e., they were not pre-bundled using pallet straps. Our maintenance efforts indicated that the branches and straps required maintenance about once every four to six months at the GTM where crepe myrtle branches were used due to both shipworm infestation (Bersoza Hernandez and Angelini, 2019) and dislodgement from vessel wakes. Through our field observations, the functional life expectancy of the GTM breakwalls was estimated to be 12 - 18 months for the branch bundles, while the life expectancy of those at NP was observed to be less than a year due to easier dislodgement of the branch fill in absence of bundling. Our observations also indicate that the fence posts were still stable after three years at both sites.

The carbon footprint of the initial construction of the nine breakwall sections at the GTM is estimated to be 2.03 metric tons of CO_2. This estimate is based solely on the gasoline required to harvest the crepe myrtle branches, transport branches and fence posts to the field sites, and construct the breakwalls (~228 gallons of unleaded gasoline; https://www.epa.gov/energy/greenhouse-gases-equivalencies-calculator-calculations-and-references). This estimate does not include the carbon cost of manufacturing and delivering the fence materials to the laboratory in Gainesville, FL, nor does it include the cost of maintaining the breakwalls or monitoring the progress of the experiment. We are not able to estimate the carbon footprint of the construction of the breakwalls at NP because information regarding the required amount of vehicle transportation of personnel and materials is unavailable. However, we estimate that the carbon footprint of the NP breakwall construction to be less than that of the GTM breakwalls because materials and volunteers were drawn from local sources, whereas all materials and labor for the GTM breakwalls had to commute from Gainesville, FL to the field sites, a round-trip distance of 251 km.

The porosities of the breakwalls from both sites were estimated by measuring the volume displaced when breakwall sections were sunk in water containers and calculating void spaces within the breakwalls. The porosity of the breakwall at GTM was obtained as $n = 0.7$ (Sections 2.3 and 4). This porosity is consistent with the results of the image processing done on these breakwalls at GTM (Herbert et al., 2018). The breakwalls built at NP, given their major differences from GTM in application (e.g., no bundling or strapping; Figure 2b), exhibited a greater porosity of $n = 0.9$.

The hydrodynamic data sets for GTM were collected during a field experiment conducted between March 29th and April 10th in 2018. Four acoustic Doppler velocimeters (Nortek Vector, with 6 MHz acoustic frequency) were located on a cross-channel array that spanned about 12.7 m (Figure 3a) west of Pine Island across the Tolomato River (ICW) at GTM (Figure 1). The velocimeters sampled pressure, three-dimensional flow velocity (East-North-Up coordinates), acoustic backscatter, and temperature at 8 Hz frequency continuously for the 13-day duration of the experiment. Using this sampling rate, the most common wakes in the data sets here (Section 3) were resolved with about 15 data points in time. A schematic of the cross-channel array, and the locations of the four velocimeters (these four locations are named G1, G2, G3, and G4 from offshore to onshore) are shown in Figure 3a. A breakwall was located between the two onshore sites G4 and G3. The mean water depths at the sites G1, G2, G3, and G4 during the experiment were 1.31 m, 1.34 m, 0.81 m, and 0.55 m, respectively (Table 1). The sensor at G4 became emerged at low tide (Figure 3a). At the location of the deployment, the river channel is about 150 m wide (Figure 1). Meteorological data collected by the GTM (NERRS, 2019) showed that winds had speeds less than 8 m/s throughout this experiment, with winds from the west (cross-channel direction with the largest fetch of 150 m for the site) being weaker than 4 m/s. These wind conditions, the limited fetch, and the analysis of the field observations altogether showed that the wind wave energy contribution to the observed waves was negligible.

At NP, the cross-channel array of the instruments spanned about 26.8 m across the Halifax River (ICW) channel (Figures 1 and 3b). At the location of the deployment, the river channel is about 140 m wide. The hydrodynamic data sets were collected on this array using three velocimeters (these three locations are named N1, N2, and N3 from offshore to onshore; Figure 3b) which sampled at 8 Hz frequency continuously between April 23rd and May 9th in 2019. The mean water depths at the sites N1, N2, and N3 during the experiment were 1.32 m, 0.60 m, and 0.50 m, respectively (Table 2). Like GTM, a breakwall was located between the two onshore sites N3 and N2. Winds were weaker than 5 m/s throughout the experiment, with westerly winds having speeds of 3 m/s maximum.

2.2 Data analysis

Boat wakes are transient and associated with relatively short timescales (minutes) compared to wind waves that can be treated as stationary over much longer timescales (hours). In the field observations, these wakes are identified as a *'chirp'* signal where the peak frequency increases in time. Therefore, advanced time-frequency analysis methods are necessary to obtain the wake parameters (energy, height, period) and statistics. In this study, the effects of tides in the data sets were filtered out by first applying a direct Fourier transformation on the entire pressure signal measured near the sea bed, then applying an inverse Fourier transformation only for frequencies that included the boat wakes and lower frequency infragravity waves. To identify the boat wakes, a windowed Fourier transform and wavelet transform were applied to the de-tided data. These steps produced spectrograms for GTM and NP data sets (Section 3) at 128 frequencies with a frequency resolution of 0.03125 Hz. Boat wakes were identified in these spectrograms due to their chirp structure and monotonically increasing frequency (e.g., Pethiyagoda et al., 2017). For each wake, the de-tided data measured near the bed were corrected for dissipation with depth (detailed below in Equations 2 and 3; Dean and Dalrymple , 1991) and the sea surface elevation was obtained. For further details on the data analysis methods, the reader is referred to Sheremet et al. (2013), Didenkulova et al. (2013), and Torsvik et al. (2015).

Wave energy flux (F) is commonly used for quantifying the eroding effects of waves on shallow systems and salt marshes like the study sites herein (e.g., Mcloughlin et al., 2015; Wiberg et al., 2015). Wave energy flux also takes depth variations and wave shoaling into account. Therefore, performances of the breakwalls in dissipating and transmitting wave energy were examined in this study by analyzing the time-frequency distribution of the wave energy flux onshore and offshore of the breakwalls. Wave energy flux in the direction of wave propagation per unit width integrated throughout the water column within a time segment of interest is obtained as in Dean and Dalrymple (1991):

$$F(x) = \int_{0}^{t} \int_{-h}^{\eta} p_D u \, dz dt \,, \tag{1}$$

where x is the coordinate of horizontal direction of wave propagation, t is time, η is sea surface elevation, h is the water depth, p_D is dynamic pressure, u is horizontal velocity, z is the vertical coordinate which is equal to zero at the surface and -h at the bed, and:

$$p_D = \rho g \frac{H}{2} \frac{cosh\, k(h+z)}{cosh\, kh} cos(\omega t + \varphi) \,, \tag{2}$$

$$u = \frac{gk}{\omega} \frac{H}{2} \frac{cosh\, k(h+z)}{cosh\, kh} cos(\omega t + \varphi) \,, \tag{3}$$

where ρ is the density of water, g is the gravitational acceleration, H is the wave height, k is the wavenumber, ω is the angular frequency of the wave (equal to $2\pi f$ where f is the frequency), and φ is the phase. Equations 1-3 show that wave energy flux is proportional to the square of wave height, i.e., $F \alpha H^2$. The cross-shore variation of wave energy flux is estimated as:

$$\frac{dF(x)}{dx} = -\kappa F(x) \,, \tag{4}$$

where κ is the rate of net change in wave energy flux in the cross-shore. In the convention of Equation 4, $\kappa > 0$ represents net dissipation, and $\kappa < 0$ represents net growth. In the discussions below, the coefficient of wave transmission (K_T) through the breakwall is used, which is obtained as:

$$K_{T,data} = \sqrt{\frac{F_t}{F_i}}, \tag{5}$$

where F_i is the incident wave energy flux estimated at the sensor just offshore of the breakwall and F_t is the transmitted wave energy flux estimated at the sensor just onshore of the breakwall.

2.3 Theory on wave transmission through breakwaters

Some studies on wave transmission through breakwaters do not take into account the effect of breakwater porosity and relate wave transmission process to water depth, breakwater geometry (such as height and width of the breakwater crest) and wave height and period (e.g., Seelig , 1980; van der Meer and Daemen, 1994; d'Angremond et al., 1996; Seabrook and Hall, 1998; van der Meer et al., 2005). These earlier studies provided empirical relations for wave transmission rates that include coefficients calibrated using laboratory data.

In studies that take the porosity of the breakwater into account, the resistance on unsteady flow through porous media is most commonly assumed to be governed by the following equation which extended Darcy's law (Darcy, 1856) by including a quadratic term (e.g., Forchheimer, 1901; Ergun and Orning, 1949; Irmay, 1958; Sollitt and Cross, 1972; Burcharth and Andersen, 1995):

$$-\frac{\partial p}{\partial x} = \rho\left(\alpha + \beta u\right) u\,, \qquad (6)$$

where the term on the left-hand side is horizontal gradient of pressure p, u is horizontal velocity, and α and β are obtained as (e.g., Engelund, 1953; Bear et al., 1968; Burcharth and Andersen, 1995):

$$\alpha = \alpha_o \frac{(1-n)^3}{n^2}\frac{\nu}{d^2}\,, \qquad (7)$$

$$\beta = \beta_o \frac{1-n}{n^3}\frac{1}{d}\,, \qquad (8)$$

where α_o and β_o are non-dimensional drag coefficients for linear and nonlinear friction terms, respectively; n is the porosity of the medium which is the ratio of the volume occupied by the fluid phase to the total volume (Section 2.1); ν is the kinematic viscosity of the fluid and d is a representative diameter of the material in the porous medium. The first term on the right-hand side of Equation 6, the linear term, denotes the laminar friction and the second term, which is nonlinear, denotes the turbulent friction. Linearizing the right-hand side of Equation 6 as:

$$(\alpha+\beta u)\,u = f_w \frac{\omega}{n} u\,, \tag{9}$$

allows derivation of a friction factor f_w as:

$$f_w = \frac{n}{kl}\left[-\left(1-\frac{kl\alpha}{2\omega}\right)+\sqrt{\left(1+\frac{kl\alpha}{2\omega}\right)^2+\frac{16\beta}{3\pi}a_i\frac{l}{h}}\right]\,, \tag{10}$$

where l is the width of the porous medium and a_i is the amplitude of the incident wave, half of the height of the incident wave H_i. Then, the rate of wave transmission, in terms of wave height, is obtained as:

$$K_{T,theory} = \frac{H_t}{H_i} = \frac{1}{1+\lambda}\,, \tag{11}$$

where H_t is the height of the transmitted wave and:

$$\lambda = \frac{kl\,f_w}{2n} = \frac{1}{2}\left[-\left(1-\frac{kl\alpha}{2\omega}\right)+\sqrt{\left(1+\frac{kl\alpha}{2\omega}\right)^2+\frac{16\beta}{3\pi}a_i\frac{l}{h}}\right]\,. \tag{12}$$

For further details of the governing equations and the derivation, see Madsen (1974). This theoretical expression for wave transmission rate depends on water depth, wave characteristics (height and frequency), geometry and material characteristics (crest width, porosity) of the porous media (a breakwall in this study) and empirical drag coefficients α_o and β_o. These two coefficients vary with the flow conditions and properties of the porous media; the average values are on the order of α_o=1140 and β_o=2.7. For compilations of ranges of these coefficients in different studies in literature, the reader is referred to van Gent (1995), Lin and Karunarathna (2007), Losada et al. (2016) and Vilchez et al. (2016). Reviews on the interaction of waves with porous media listed the limited range of field observations on this interaction as the biggest knowledge gap and displayed the need for further research on transmission of waves through porous structures made of different material properties in different flow conditions (Chwang and Chan, 1998; Losada, 2001; Losada et al., 2016).

3 Results

Nearly 1000 boat wakes and their wake propagation were detected in the two two-week-long experiments at GTM and NP. A three-hour-long time series of pressure measurements at the GTM site G4 is shown in Figure 4a. Tides at the GTM were dominantly semi-diurnal with a range of 1 - 1.5 m; tides at NP were also semi-diurnal but with a smaller range of 0.2 - 0.3 m. The effects of tides (thick red line in Figure 4a) were filtered out to obtain the de-tided data shown in Figure 4b. As an example, the spectrogram obtained from the windowed Fourier transform (Figure 4c) for the wake identified at the GTM site G4 on March 30th at 0900 hours is shown in Figure 5a. The chirp structure and monotonically increasing frequency of the wake are prominent. Correction on the pressure measurements for dissipation with depth gives the sea surface elevation (Equation 2; Figure 5b). Using sea surface elevation, vertical structures of wake-induced pressure fluctuations and orbital velocities throughout the entire water column were reconstructed based on linear wave theory (Equations 2 and 3; Figure 6). The orbital velocities and the dynamic component of pressure were used in estimating wave energy flux (Section 2.2; Equation 1).

The wakes were classified in the database together with the height of the highest wave in each wake and the corresponding frequency of that wave. The data set at the GTM captured 290 wakes (Figure 7). The number of wake events at the NP data set, which is of longer duration compared to GTM data set (17 days vs. 13 days) and was collected closer to summer (early May vs. early April) is much higher than the number of wake events at the GTM (673 wake events; Figure 8). At GTM, the wake heights reached 1 m at the offshore sites and 0.6 m onshore of the breakwall with wave periods sometimes exceeding 5 s (Figure 7). The distributions of wake heights and periods onshore of the breakwall at NP are similar to those at GTM in the sense that the wakes most commonly had periods of 1.5-2 s and heights less than or equal to 0.1 m (55% of wake events) while the heights sometimes exceeded 0.5 m (Figure 8). Boat wakes with periods of ~2 s most frequently but reaching 5 s occasionally represent the common conditions observed in intracoastal waterways like the study site here (Sheremet et al., 2013; Didenkulova et al., 2013). The distributions of the wakes captured at the GTM experiment show a noticeable decrease in wave height just onshore of the breakwall compared to those just offshore of the breakwall (Figure 7). In contrast, the frequency distributions of the wake heights and periods onshore and offshore of the breakwall at NP are relatively similar (Figure 8).

The performance of the breakwalls in dissipating and transmitting wave energy was examined by analyzing the time-frequency distribution of the wave energy flux (Section 2.2; Equations 1-5). Overall, transmission shows an increasing trend with increasing water levels at both sites; however, the rates of transmission are quite different at the two sites (Figures 9 and 10). The results of the analysis on the GTM data set show that the breakwall at the GTM transmitted between 9% and 85% (less than 70% transmission in 87% of the events) of the incoming wave energy flux (Figure 9). The rate of transmission averaged over all wake events is 53%. Transmission rates have an increasing trend with increasing water levels (up to depths of ~1.1 m; Figure 9). This field observation of such dependency of transmission rates on tidal variations agrees with the findings from experiments of waves being dissipated by oyster reefs in shallow bays (Wiberg et al., 2019), results at a comprehensive database of laboratory experiments on wave transmission through submerged structures (van der Meer et al., 2005), and results of related numerical simulations (Ting et al., 2004). The height of the breakwall structure (h_s) and water depth (h) are critical for engineering and related guidelines, therefore, the variation of wave transmission in relation to these two parameters is also evaluated. The influence of the height of the breakwall structure relative to water depth (h_s/h) on wave transmission is evident at shallower depths, especially for h_s/h varying between h_s/h~0.5 and h_s/h~1 which correspond to mid-tide and low-tide conditions here, respectively (Figure 9). However, the variations in transmission rates are much smaller at higher depths (h_s/h<0.5) at high-tide. Both of these observations are consistent with the findings of Losada et al. (1996) and Lin and Karunarathna (2007).

The results of the analysis on the NP data show also an overall increasing trend of wave transmission with increasing water levels (Figure 10). Comparing the results from the analysis on the wakes measured at the NP to those at the GTM indicates a strikingly different pattern of wave transmission, with much greater wave transmission rates through the higher porosity breakwall design at NP (Figure 10): almost all wake events at NP had transmission rates between 70% and 100%; the rate of transmission averaged over all wake events is 83%. Due to the smaller tidal range at NP compared to GTM, the breakwall at NP emerged during almost the entire experiment at that site (Figure 2b), and much more often than the one at GTM which was fully submerged more than half of the experiment at that site (Figure 2a). Therefore, if the two breakwalls had been built the same way (e.g., bundling, porosity), the NP breakwall would have been more likely to dissipate more wave energy and transmit less (Wiberg et al., 2019). However, the average rate of transmission at NP (83%) is much greater than the one at GTM (53%). This can be attributed to the difference in design at NP, i.e., individual tree branches were not pre-bundled before being secured within the fence post wall frame, contributing to the greater porosity of the breakwall at this site (Section 2.1). The other difference evident from the results for NP compared to GTM is the much less variability of wave transmission rates with tides (Figure 10), which could be due to the smaller tidal range at NP, and with h_s/h. The binned-averages over depth ranges all give transmission rates that are very close to the overall average of ~83% for the NP breakwall (Figure 10).

4 Discussion

Observations and analyses of the interaction of hydrodynamics with two types of living shoreline breakwalls (Section 3) show different wave transmission patterns and rates that are modulated by tides and breakwall porosity. Overall, these results support the hypotheses of this study that semi-porous living shoreline breakwalls help reduce wave energy, and their performance is dependent on depth variations. For the GTM experiment, where wave transmission through the breakwall was observed to be strongly modulated by tides (Figure 9), the estimates based on the field observations (Section 2.2; Equation 5) and theoretical estimates of wave transmission (Section 2.3; Equation 11) are evaluated using the relative discrepancy between them:

$$\varepsilon = \frac{K_{T,theory} - K_{T,data}}{K_{T,data}} \,. \tag{13}$$

Considering the uncertainties in both the estimates based on the field data and the theoretical estimates, ε is treated here as a discrepancy, rather than error. The sensitivity analysis showed that the theoretical estimates are not sensitive to the laminar friction coefficient (i.e., α_o; Equations 6-12). As a result, α_o=1140, the median value of the most common range given in the literature for this coefficient (780 - 1500) is used here. The optimum value for turbulent friction coefficient (i.e., β_o; Equations 6-12) is obtained by minimizing the absolute relative discrepancy averaged over all 290 wake events ($\overline{|\varepsilon|}$). This is satisfied with an optimum turbulent friction coefficient of β_o=2.7 (Figure 11), which is consistent with the literature on waves through porous media (Section 2.3).

Theoretical transmission rate ($K_{T,theory}$) estimated using the optimum β_o=2.7 captures the measured transmission with $\overline{|\varepsilon|}$=16% on average for all 290 wake events at the GTM (Figure 11). Using β_o=2.7 also maximizes the number of wake events with absolute relative discrepancy ($|\varepsilon|$) less than 10% and 20% (Figure 11). $|\varepsilon|$ is less than 10% in half of the wake events, less than 20%

in 70% of the wake events, and less than 30% in 90% of the wake events. Estimated transmission in 10% of the wake events has $|\varepsilon|$ greater than 30%. These wake events with relatively high discrepancy correspond to shallow depth conditions and h_s/h~1 such that the breakwall was getting close to be emerged (Figure 12). The discrepancy in those cases is due to the overestimation of the transmitted wave energy by the theory (Figure 12). This is attributed to the dissipative processes that are not accounted for in the theoretical analysis but become relatively important in shallow water, such as breaking and bottom friction. The fact that this discrepancy is due to an overestimation by theory is comforting in terms of the use of this theoretical approach towards desired dissipation of waves by sufficiently engineered living shorelines.

At NP where variability in transmission was relatively small, average observed transmission rate is ~0.83 (Section 3) which is equivalent to $K_{T,data}$~0.911 (Equation 5) in terms of wave height transmission through the breakwall. The theoretical estimate of wave height transmission for the breakwall at NP is obtained from Equations 7-12. Using the breakwall properties (geometry, porosity) and the common wave conditions observed at NP, and the friction coefficients obtained from the theoretical analysis above (α_o=1140; β_o=2.7) that are also consistent with the literature on waves through porous media, the theoretical estimate is obtained as $K_{T,theory}$~0.906 which is very close to the observed transmission ($K_{T,data}$).

5 Conclusions

The performance of living shorelines in dissipating wave energy was studied here in intertidal settings. To the best of the authors' knowledge, this study is the first evaluation of wave transmission through living shoreline breakwalls using field observations, suitable data analysis methods, and theoretical approaches. The settings of interest were inner coastal and estuarine areas along navigation channels that are common around the world, including along US East and Gulf coasts. Fetch distances in these areas are commonly small and wave climate is dominated by boat wakes due to high recreational and navigational traffic. Accordingly, transmission of boat wakes through porous breakwalls composed of tree branches and fence posts were investigated by collecting field measurements of wake propagation, analyzing these data sets using time-frequency methods, and comparing the findings to available theory on hard engineering structures. The observations highlighted the intensity of boat traffic on the ICW and the dynamics of boat wake climate in this system.

The results of the analyses on the two breakwall configurations tested revealed different behaviors of wave transmission. In the first breakwall design with a porosity of 0.7, where tree branches were bundled to the fence posts, transmission rates were found to vary mostly between 9% and 70% and be directly proportional to water depth, especially at mid-tide and low-tide conditions where the height of the breakwall relative to water depth was between 0.5 and 1. In the second breakwall design with a higher porosity of 0.9 where the branches were not bundled, wave transmission rates exceeded 70% in 84% of the cases, sometimes reaching 100%, and showed much less variability with tides. These results support our hypotheses that well-engineered living shoreline breakwalls can be used as buffers against human-mediated boat traffic and waves, and their related performance in dissipating wave energy and sustaining coastal ecosystems is modulated by depth and porosity.

Theoretical estimates of wave transmission through the breakwalls were found to be most sensitive to breakwall porosity and turbulent friction coefficient. A turbulent friction coefficient of 2.7, a value which is the median of the most common range given in the literature on wave transmission through rubble mound breakwaters, gave the best agreement between the observation-based estimates and theoretical estimates of wave transmission. This study also showed that the theory on wave transmission through porous media can be applied to the interaction of waves with porous living shorelines. The highest discrepancy between observed and theoretical estimates of wave transmission was found at relatively shallow depth conditions when the breakwall began to emerge. In these cases, the theory was found to overestimate transmitted wave energy. This overestimation is possibly due to breaking and bottom friction processes which become more important in shallow waters, but are not accounted for in the theoretical analysis of wave transmission. Such living shorelines can be essential for protecting and sustaining coastal wetlands and reefs and supporting shoreline integrity along locations where wave energy is high. The major factors to consider regarding the applicability of this living shoreline concept at other sites are proximity and abundance of locally available material and labor, ease of access for maintenance and monitoring, sediment features (Safak et al., under review), and local abundance of bioeroding organisms. In terms of waves and hydrodynamics, the observational and theoretical results in this study could be used as first-cut guidelines toward exporting this living shoreline design to other sites with different meteorological and hydrodynamic conditions and estimating the wave transmission through these nature-based structures with a given wave climate, water depth range, and breakwall properties.

Acknowledgments

This work was sponsored by the National Estuarine Research Reserve System Science Collaborative, which supports collaborative research that addresses coastal management problems important to the reserves. The Science Collaborative is funded by the National Oceanic and Atmospheric Administration and managed by the University of Michigan Water Center (NAI4NOS4190145). This research was also funded by the Florida Fish and Wildlife Conservation Commission (FWC) through the Florida Marine Resources Trust Fund allocated during the 2018-2019 fiscal year. Living shoreline installations were conducted by GTM National Estuarine Research Reserve, FWC, North Peninsula State Park, and St.Johns River Water Management District staff and volunteers. Support from Todd Van Natta from the University of Florida, Ron Brockmeyer from the St. Johns River Water Management District, Dr. Joe Calantoni and his staff from the Naval Research Laboratory are acknowledged. We would like to thank the Associate Editor Dr. Agustin Sanchez-Arcilla and the two reviewers for the time and effort they spent for providing suggestions towards improving the manuscript.

Conflicts of interest

The authors declare no conflicts of interest.

References

Bauer, G., Lorang, M.S., Sherman, D.J., 2002. Estimating boat-wake-induced levee erosion using sediment suspension measurements. J. Waterw. Port Coas. Ocean Eng. 128(4), 152-162.

Bear, J., Zaslavsky, D., Irmay, S., 1968. Physical principles of water percolation and seepage. UNESCO SC.NS.65/III.34/A. 465 p. https://unesdoc.unesco.org/ark:/48223/pf0000070033

Bersoza Hernandez A, Angelini C (2019) Wood traits and tidal exposure mediate shipworm infestation and biofouling in southeastern U.S. estuaries. Ecolog. Eng. 132, 1-12.

Bilkovic, D.M., Mitchell, M., Mason, P., Duhring, K., 2016. The role of living shorelines as estuarine habitat conservation strategies. Coas. Manag. 44, 161–174.

Boumans, R.M.J., Day, J.W., Kemp, G.P., Kilgen, K., 1997. The effect of intertidal sediment fences on wetland surface elevation, wave energy and vegetation establishment in two Louisiana coastal marshes. Ecolog. Eng. 9, 37–50.

Bulte, G., Carriere, M.-A., Blouin-Demers, G., 2010. Impact of recreational power boating on two populations of northern map turtles (Graptemys geographica). Aquatic Conserv: Mar. Freshw. Ecosyst. 20, 31–38.

Burcharth, H.F., Andersen, O.H., 1995. On the one-dimensional steady and unsteady porous flow equations. Coas. Eng. 24, 233–257.

Chwang, A.T., Chan, A.T., 1998. Interaction between porous media and wave motion. Ann. Rev. Fluid Mech. 30, 53-84.

Dalrymple, R.A., Losada, M.A., Martin, P.A., 1991. Reflection and transmission from porous structures under oblique wave attack. J. Fluid Mech. 224, 625-644.

Darcy, H.P.G., 1856. Les fontaines publiques de la ville k Dijon, Exposition et application des principes & suivre et des formules d employer dans les questions dt distribution d'eau, Victor Dalmont, Paris, 647 p.

d'Angremond, K., van der Meer, J.W., de Jong, R.J., 1996. Wave transmission at low-crested structures. Proc. 25th Int. Conf. Coas. Eng., ASCE, 2418–2427.

Davenport, T.M., Seitz, R.D., Knick, K.E., Jackson, N., 2018. Living shorelines support nearshore benthic communities in upper and lower Chesapeake Bay. Estuar. Coas. 41, S197-S206.

Davis, J.L., Currin, C.A., O'Brien, C., Raffenburg, C., Davis, A., 2015. Living shorelines: coastal resilience with a blue carbon benefit. PLoS ONE 10 (11): e0142595. doi:10.1371/journal.pone.0142595

Dean, R.G., Dalrymple, R.A., 1991. Water Wave Mechanics for Engineers and Scientists, reprinted Singapore. World-Scientific Publishing Co.

Didenkulova, I., Sheremet, A., Torsvik, T., Soomere, T., 2013. Characteristic properties of different vessel wake signals. J. Coas. Res. 65, 213–218.

Dugan, J.E., Hubbard, D.M., Rodil, I.F., Revell, D.L., Schroeter, S., 2008. Ecological effects of coastal armoring on sandy beaches. Mar. Eco. 29, 160–170.

Ellis, J.T., Sherman, D.J., Bauer, B.O., Hart, J., 2002. Assessing the impact of an organic restoration structure on boat wake energy. J. Coas. Res., SI 36, 256–265.

Engelund, F., 1953. On the laminar and turbulent flow of ground water through homogeneous sand. Trans. Dan. Acad. Tech. Sci., 3, No. 4.

Ergun, S., Orning, A.A., 1949. Fluid flow through randomly packed columns and fluidized beds. Industr. Eng. Chem. 41, 1179–1184.

Florida Department of Environmental Protection, 2018. Critically eroded beaches in Florida. Division of Water Resource Management, 89 p. https://floridadep.gov/sites/default/files/CriticallyErodedBeaches.pdf ; https://ca.dep.state.fl.us/mapdirect/?focus=beaches

Florida Highway Safety and Motor Vehicles, 2012. Vessel owners: Statistics 2011. Florida Department of Highway Safety and Motor Vehicles. http://www.flhsmv.gov/dmv/vslfacts.html.

Forchheimer , P., 1901. Zeits. d. Verein Deutsch. Ing. 45, 1782.

Gabel, F., Lorenz, S., Stoll, S., 2017. Effects of ship-induced waves on aquatic ecosystems. Sci. Total Environ. 601-602, 926–939.

Herbert, D., Astrom, E., Bersoza, A.C., Batzer, A., McGovern, P., Angelini, C., Wasman, S., Dix, N., Sheremet, A., 2018. Mitigating erosional effects induced by boat wakes with living shorelines. Sustainability 10 (2), doi: 10.3390/su10020436

Irmay, S., 1958. On the theoretical derivation of Darcy and Forchheimer formulas. Trans. Amer. Geophys. Union 39 (4), 702-707.

Jackivicz, T.P., Kuzminski, L.N., 1973. The effects of the interaction of outboard motors with the aquatic environment—A review. Environ. Res. 6(4), 436–454.

Keddy, P.A., 1982. Quantifying within-lake gradients of wave energy: Interrelationships of wave energy, substrate particle size and shoreline plants in Axe Lake, Ontario. Aquatic Botany 14, 41–58.

Kraus, S. D., Brown, M. W., Caswell, H., Clark, C.W., Fujiwara, M., Hamilton, P. K., Kenney, R., Knowlton, A., Landry, S., Mayo, C. A., McLellan, V.A., Moore, M. J., Nowacek, D. P., Pabst, D.A., Read, A., Rolland, R. 2005. North Atlantic right whales in crisis. Science 309 (5734), 561-562.

Kucera-Hirzinger, V., Schludermann, E., Zornig, H., Weissenbacher, A., Schabuss, M., Schiemer, F., 2009. Potential effects of navigation-induced wave wash on the early life history stages of riverine fish. Aqua. Sci. 71, 94-102.

Lin, P., Karunarathna, S.A.S.A., 2007. Numerical study of solitary wave interaction with porous breakwaters. J. Waterw. Port Coas. Ocean Eng. 133(5): 352-363.

Losada, I.J., Silva,R., Losada, M.A., 1996. 3-D non-breaking regular wave interaction with submerged breakwaters. Coas. Eng. 28, 229-248

Losada, I.J., 2001. Recent advances in the modeling of wave and permeable structure interaction. Adv. Coas. Ocean Eng. 163-202. https://doi.org/10.1142/9789812794574_0004

Losada, I.J., Lara, J.L., del Jesus, M., 2016. Modeling the interaction of water waves with porous coastal structures. J. Waterw. Port Coas. Ocean Eng. 142(6): 03116003.

Madsen, O.S., 1974. Wave transmission through porous structures. J. Waterw. Port Coas. Ocean Eng., Proc. ASCE, 100, 169-188.

McLoughlin, S.M., Wiberg, P.L., Safak, I., McGlathery, K.J., 2015. Rates and forcing of marsh edge erosion in a shallow coastal bay. Estua. Coas. 38, 620-638.

Montes, N., Swett, R., Sidman, C., Fik, T., 2016. Offshore recreational boating characterization in the Southeast US. University of Florida Sea Grant Program, TP 226, https://www.flseagrant.org/wp-content/uploads/Tp_226_web.pdf

Morris, R.L., Konlechner, T.M., Ghisalberti, M., Swearer, S.M., 2018. From grey to green: Efficacy of eco-engineering solutions for nature-based coastal defence. Global Change Biology 24, 1827-1842.

National Oceanic and Atmospheric Administration (NOAA) National Estuarine Research Reserve System (NERRS) system-wide monitoring program. Data accessed from the NOAA NERRS

Centralized Data Management Office website: http://www.nerrsdata.org/ ; accessed May 16th, 2019.

O'Donnell, J.E.D., 2018. Living shorelines: a review of literature relevant to New England coasts. J. Coas. Res. 33, 435-451.

Parnell, K.E., McDonald, S.C., Burke, A.E., 2007. Shoreline effects of vessel wakes, Marlborough Sounds, New Zealand. J. Coas. Res. SI 50, 502-506.

Pethiyagoda, R., McCue, S.W., Moroney, T.J., 2017. Spectrograms of ship wakes: identifying linear and nonlinear wave signals. J. Fluid Mech. 811, 189–209.

Polk, M.A., Eulie, D.O., 2018. Effectiveness of living shorelines as an erosion control method in North Carolina. Estuar. Coas. 41, 2212-2222.

Price, F.D., 2005. Quantification, analysis, and management of Intracoastal Waterway channel margin erosion in the Guana Tolomato Matanzas National Estuarine Research Reserve, Florida. Master's Thesis, Florida State University, Tallahassee, FL, USA.

Safak, I., Norby, P.L., Dix, N., Grizzle, R., Southwell, M., Veenstra, J.J., Acevedo, A., Cooper-Kolb, T., Massey, L., Sheremet, A., Angelini, C., 2020. Coupling breakwalls with oyster restoration structures enhances living shoreline performance along energetic shorelines. Ecolog. Eng.

Safak, I., Angelini, C., Sheremet, A., Boat wake effects on sediment transport in intertidal waterways (under review).

Seabrook, S.R., Hall, K.R., 1998. Wave transmission at submerged rubblemound breakwaters. Proc. 26th Int. Conf. Coas. Eng., ASCE, 2000–2013.

Seelig, W. N., 1980. Two-dimensional tests of wave transmission and reflection characteristics of laboratory breakwaters. Tech. Rept. No. 80-1, U.S. Army Corps of Eng., Coas. Eng. Res. Ctr., Fort Belvoir, VA.

Seitz, R.D., Lipcius, R.N., Olmstead, N.H., Seebo, M.S., Lambert, D.M., 2006. Influence of shallow-water habitats and shoreline development on abundance, biomass, and diversity of benthic prey and predators in Chesapeake Bay. Mar. Ecol. Prog. Ser. 326, 11–27.

Sharma, S., Goff, J., Cebrian, J., Ferraro, C., 2016. A hybrid shoreline stabilization technique: Impact of modified intertidal reefs on marsh expansion and nekton habitat in the northern Gulf of Mexico. Ecolog. Eng. 90, 352-360.

Sheremet, A., Gravois, U., Tian, M., 2013. Boat wake statistics at Jensen Beach, Florida. J. Waterw. Port Coas. Ocean Eng. 139, 286-294.

Smith, C.S., Puckett, B., Gittman, R.K., Peterson, C.H., 2018. Living shorelines enhanced the resilience of saltmarshes to Hurricane Matthew (2016). Ecolog. Appl. 28, 871-877.

Sollitt, C.K., Cross, R.H., 1972. Wave transmission through permeable breakwaters. Proc. 13th Int. Conf. Coas. Eng., ASCE, 1827–1846.

Ting, C.-L., Ling, M.-C., Cheng, C.-Y., 2004. Porosity effects on non-breaking surface waves over permeable submerged breakwaters. Coas. Eng. 50, 213–224.

Torsvik, T., Soomere, T., Didenkulova, I., Sheremet, A., 2015. Identification of ship wake structures by a time–frequency method. J. Fluid Mech. 765, 229–251.

UNEP, 2007. Global outlook for ice&snow. Chapter 6c: Ice and sea-level change. United Nations Environment Programme. UNEP Job No: DEW/0924/NA

van der Meer, J.W., Daemen, I.F.R., 1994. Stability and wave transmission at low-crested rubble-mound structures. J. Waterw. Port Coas. Ocean Eng. 120 (1), 1-19.

van der Meer, J.W., Briganti, R., Zanuttigh, B., Wang, B., 2005. Wave transmission and reflection at low-crested structures: design formulae, oblique wave attack and spectral change. Coas. Eng. 52, 915-929.

van Gent, M.R.A., 1995. Porous flow through rubble-mound material. J. Waterw. Port Coas. Ocean Eng. 121, 176-181.

Vilchez, M., Clavero, M., Lara, J.L., Losada, M.A., 2016. A characteristic friction diagram for the numerical quantification of the hydraulic performance of different breakwater types. Coas. Eng. 114, 86–98.

Wall, L.M., Walters, L.J., Grizzle, R.E., Sacks, P.E., 2005. Recreational boating activity and its impact on the recruitment and survival of the oyster Crassostrea virginica on intertidal reefs in Mosquito Lagoon, Florida. J. Shellfish Res. 24(4), 965–973.

Walters, L.J., Johnson, K., Wall, L.M., Martinez, N., Grizzle, R., 2002. Shell movement and juvenile survival of the oyster on intertidal reefs adjacent to waters with intense boating activity in the Indian river Lagoon, Florida. J. Shellfish Res. 21(1), 415–416.

Wiberg, P.L., Carr, J.A., Safak, I., Anutaliya, A., 2015. Quantifying the distribution and influence of non-uniform bed properties in shallow coastal bays. Limnol. Oceanogr. - Methods 13(12), 746–762. DOI: 10.1002/lom3.10063

Wiberg, P.L., Taube, S.R., Ferguson, A.E., Kremer, M.R., Reidenbach, M.A., 2019. Wave attenuation by oyster reefs in shallow coastal bays. Estua. Coas. 42, 331-347. https://doi.org/10.1007/s12237-018-0463-y

Wolter, C., Arlinghaus, R., 2003. Navigation impacts on freshwater fish assemblages: the ecological relevance of swimming performance. Rev. Fish Bio. Fisher. 13, 63–89.

Table 1: Names and depths of the measurement sites at GTM in March-April 2018. The depth values are averages over the experiment duration.

Name	Mean depth (m)
G1	1.31
G2	1.34
G3	0.81
G4	0.55

Table 2: Names and depths of the measurement sites at NP in April-May 2019. The depth values are averages over the experiment duration.

Name	Mean depth (m)
N1	1.32
N2	0.60
N3	0.50

Figure 1: The locations of the cross-channel transects (marked with red asterisks) of the instrumented platforms at the Atlantic Intracoastal Waterway. Left and right panels show the aerial views of the locations of the GTM site west of the Pine Island along the Tolomato River and the NP site along the Halifax River, respectively. The aerial views are obtained from the United States Geological Survey EarthExplorer database. Inset map shows where the two sites are located in the State of Florida in the United States.

Figure 2: Photographs of the breakwalls at the (a) GTM and (b) NP sites. The two photographs were taken at different phases of the tide.

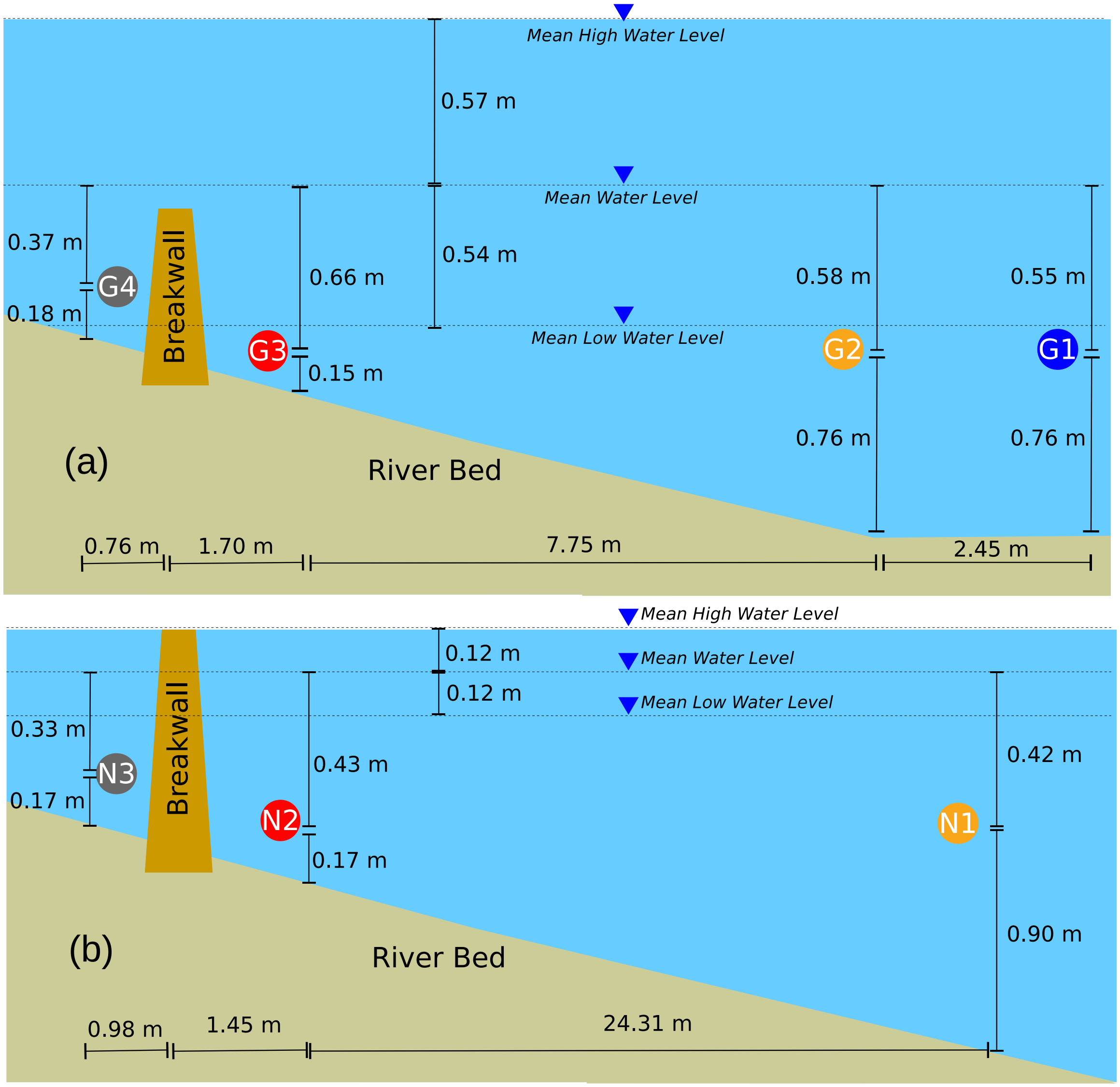

Figure 3: Cross-channel transects of the instruments deployed during the field experiments at (a) GTM between March 29th and April 10th in 2018 and (b) NP between April 23rd and May 9th in 2019. Mean tidal variations averaged over the experiment durations are also indicated. Filled circles show the locations of the pressure sensors. Vertical scales are exaggerated for clarity.

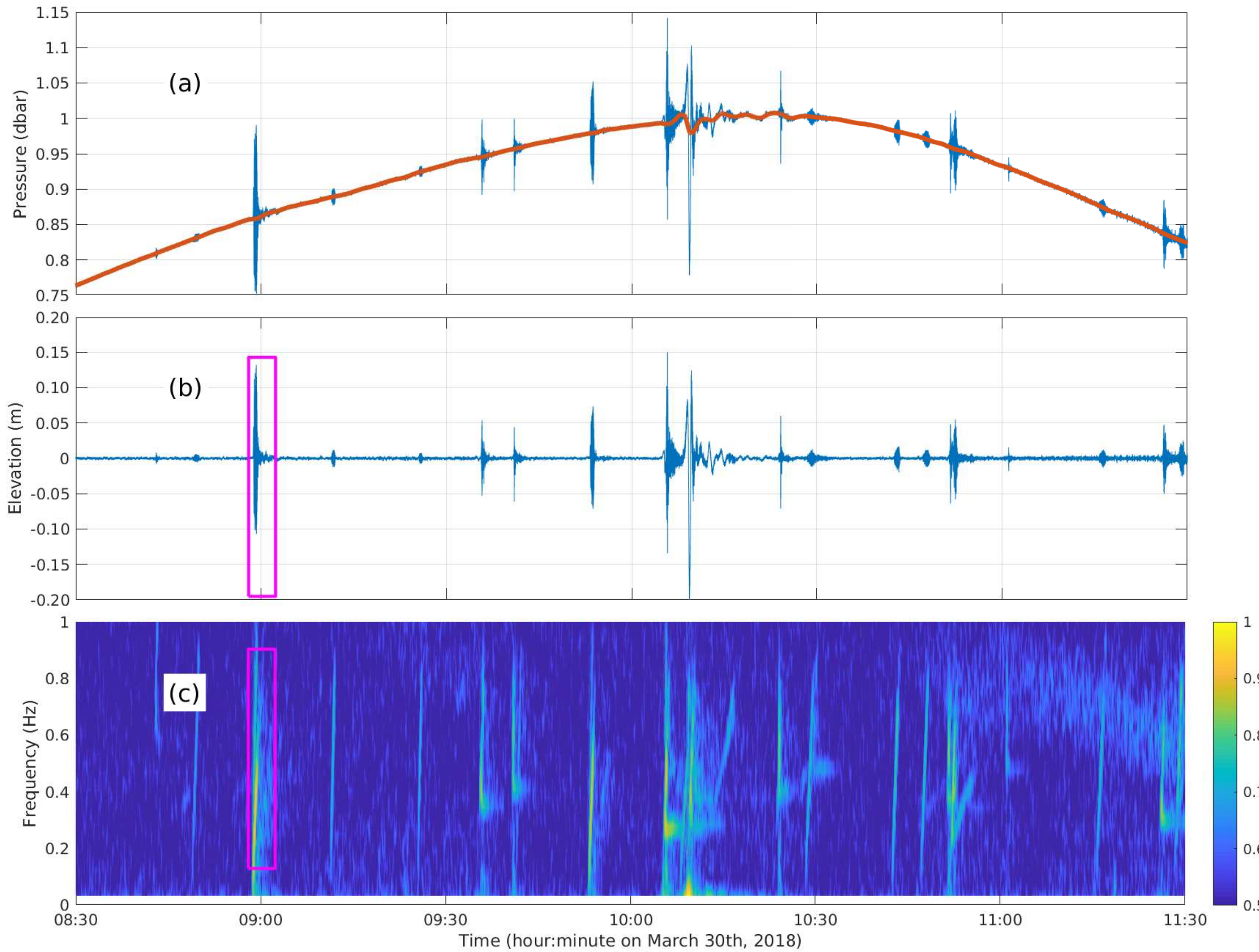

Figure 4: Three-hour-long time-series of (a) pressure measurements near bed; (b) de-tided pressure data; (c) normalized spectrogram of pressure (warm colors indicate high energy) at GTM site G4 on March 30th, 2018. The red curve in panel (a) shows the tidal signal; the magenta boxes in panels (b) and (c) mark the boat wake analyzed in detail in Figures 5 and 6.

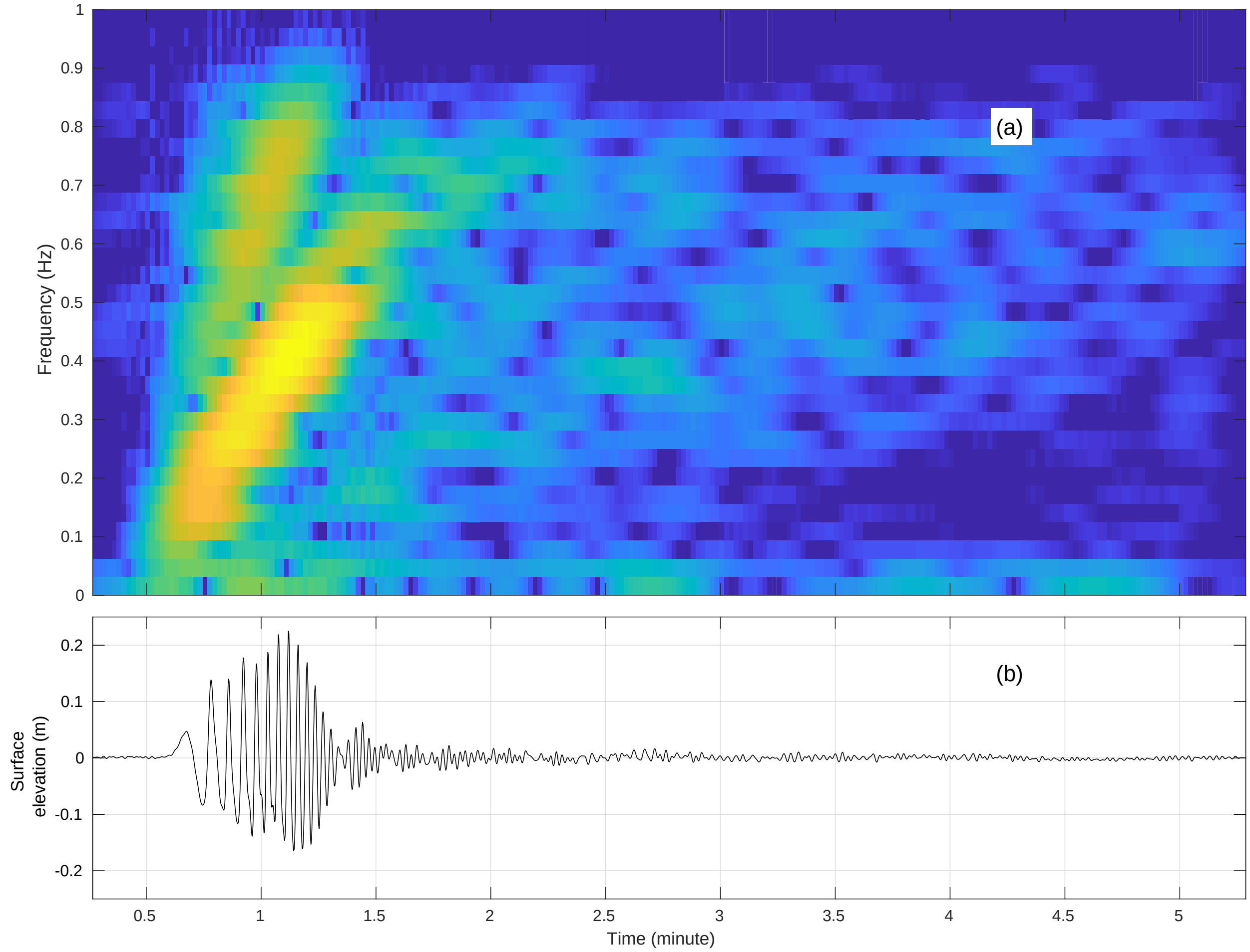

Figure 5: An example boat wake measured at the GTM site G4 on March 30th at 0900 hours. (a) Normalized spectrogram of pressure (warm colors indicate high energy), (b) sea surface elevation.

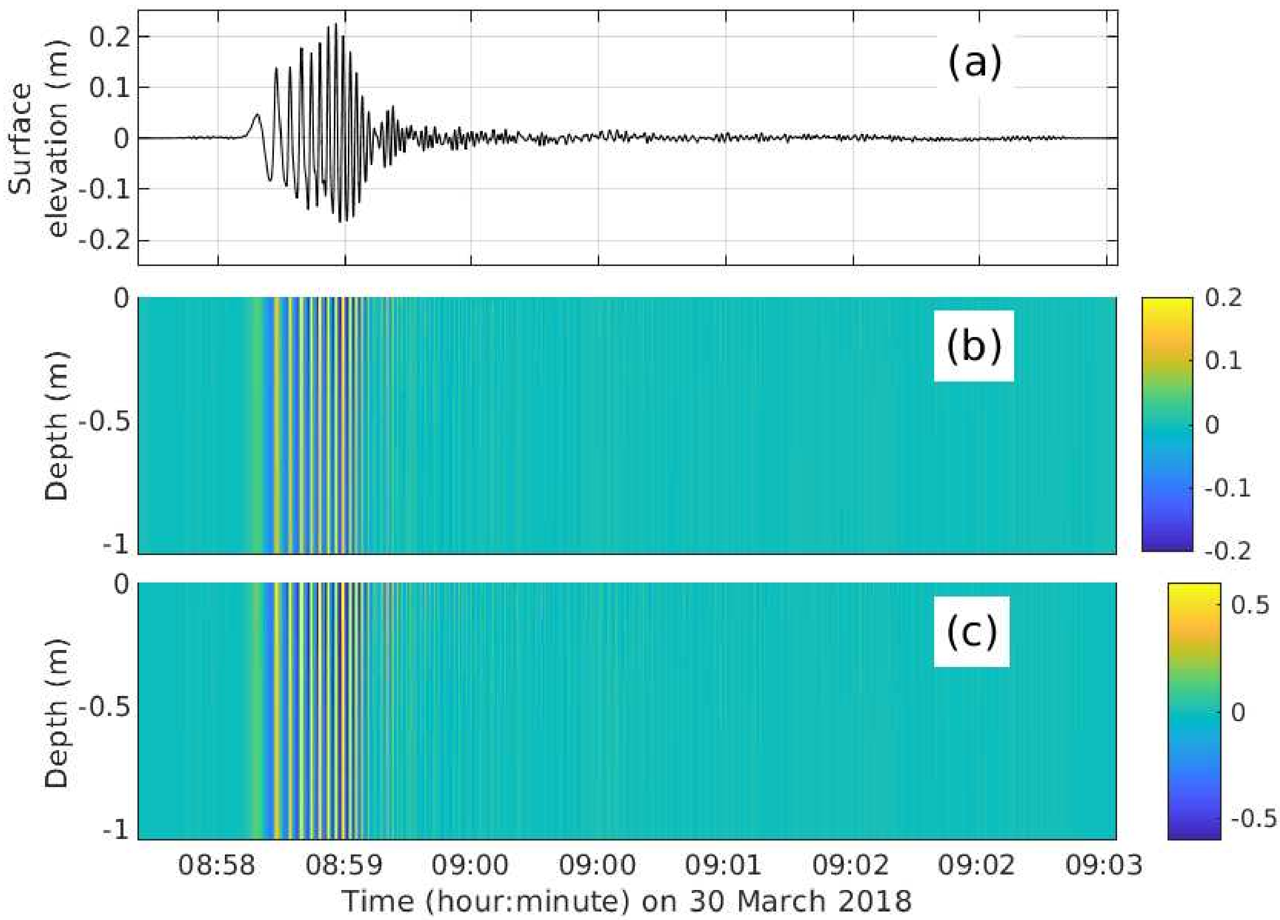

Figure 6: Flow of the boat wake at the GTM site G4 on March 30th at 0900 hours. (a) Sea surface elevation, (b) vertical structure of dynamic pressure (dbar; Equation 2), and (c) vertical structure of orbital velocity (m/s; Equation 3).

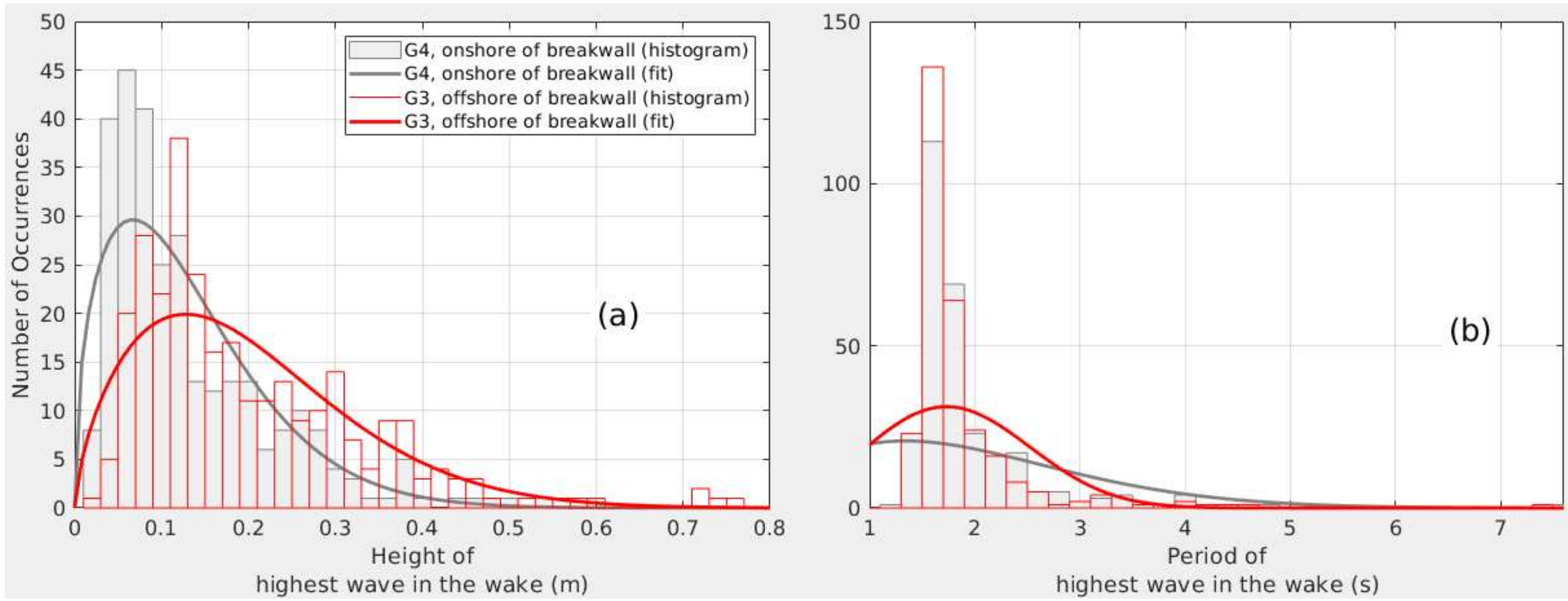

Figure 7: Histograms of (a) maximum wave height, and (b) corresponding period in each wake recorded between March 29th and April 10th, 2018 at the GTM sites G4 that was just onshore of the breakwall (grey) and G3 that was just offshore of the breakwall (red). The thick curves show the Weibull distribution fits to the histograms.

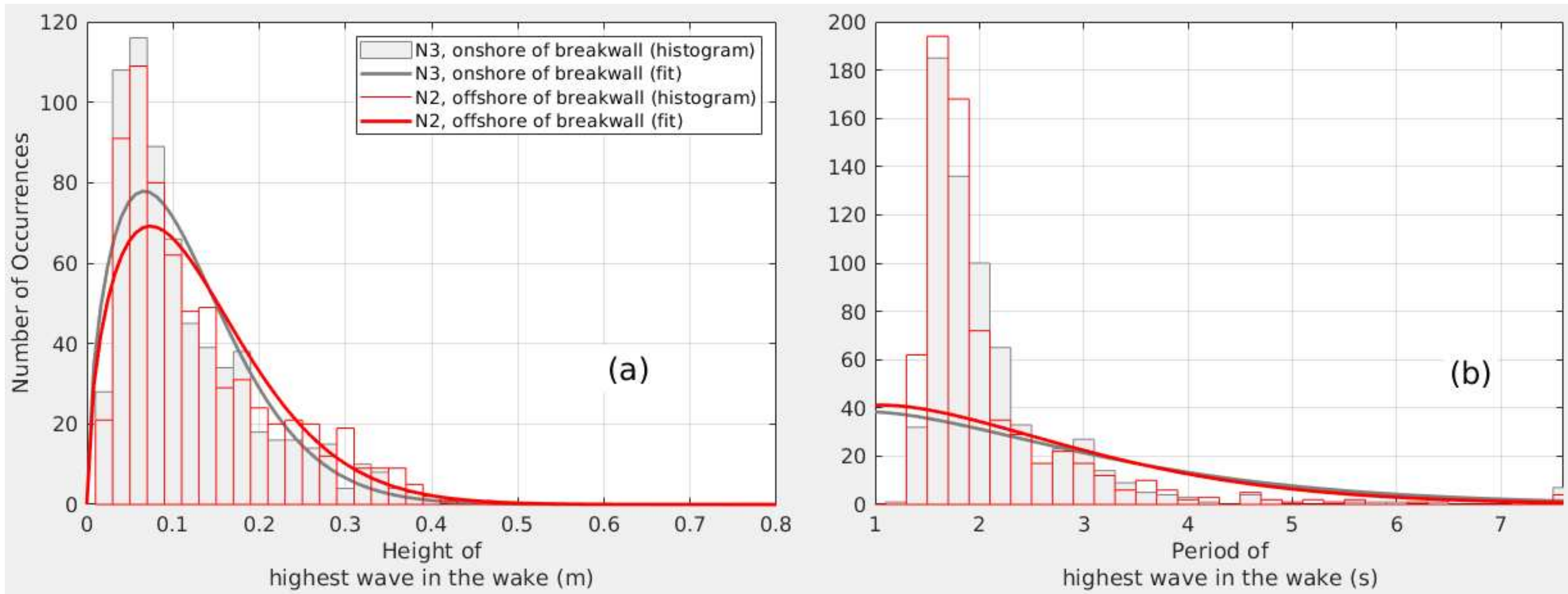

Figure 8: Histograms of (a) maximum wave height, and (b) corresponding period in each wake recorded between April 23rd and May 9th, 2019 at the NP sites N3 that was just onshore of the breakwall (grey) and N2 that was just offshore of the breakwall (red). The thick curves show the Weibull distribution fits to the histograms.

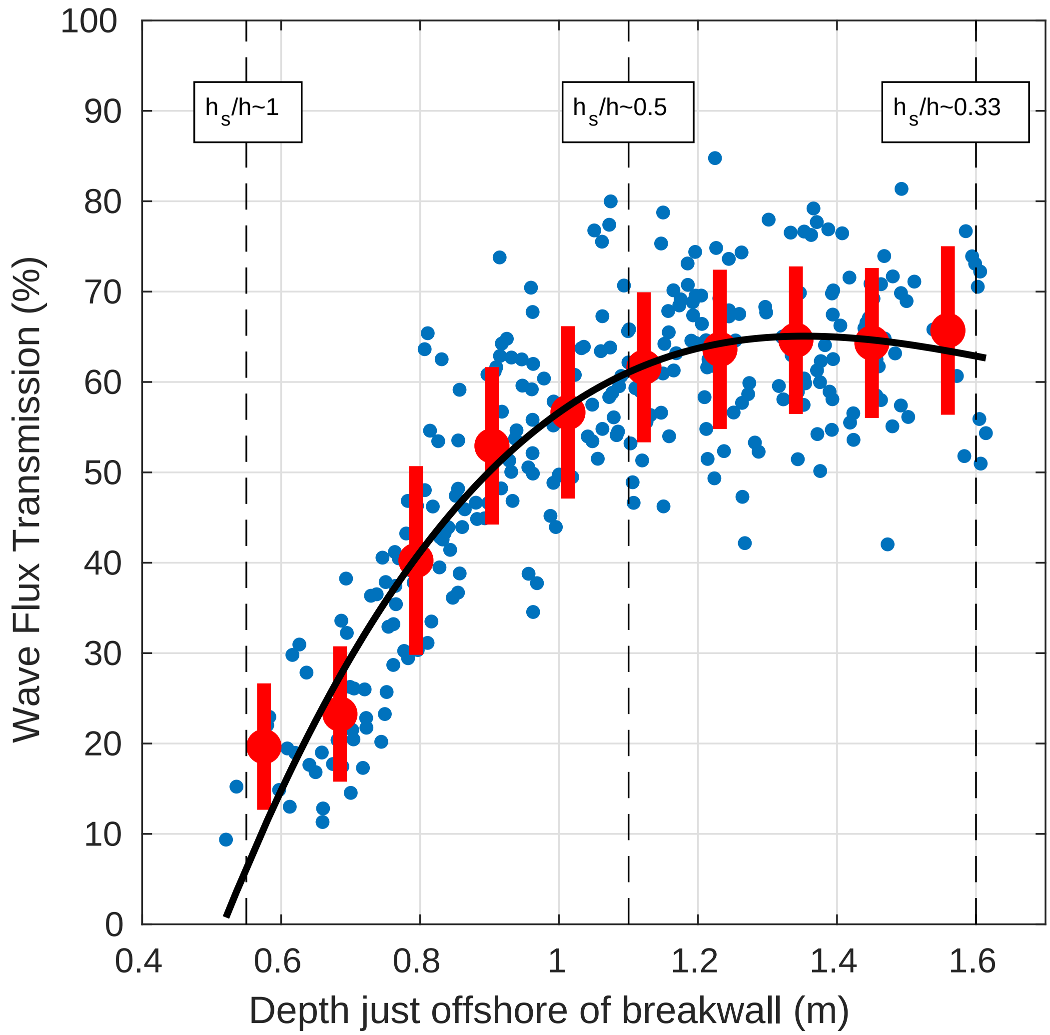

Figure 9: Rates of wave energy flux transmission from GTM site G3 (just offshore of the breakwall) to G4 (just onshore of the breakwall) as a function of depth. Blue dots are the estimates from the wake events; the big red dots are averages over 10-cm-wide depth bins; vertical red bars show $\pm$ standard deviation; the black curve is a least squares fit through the estimates. Dashed straight lines indicate the conditions the relative height of the breakwall, which is the ratio of the breakwall to water depth, is equal to 1, 0.5, and 0.33; i.e., h_s/h~1, h_s/h~0.5, and h_s/h~0.33.

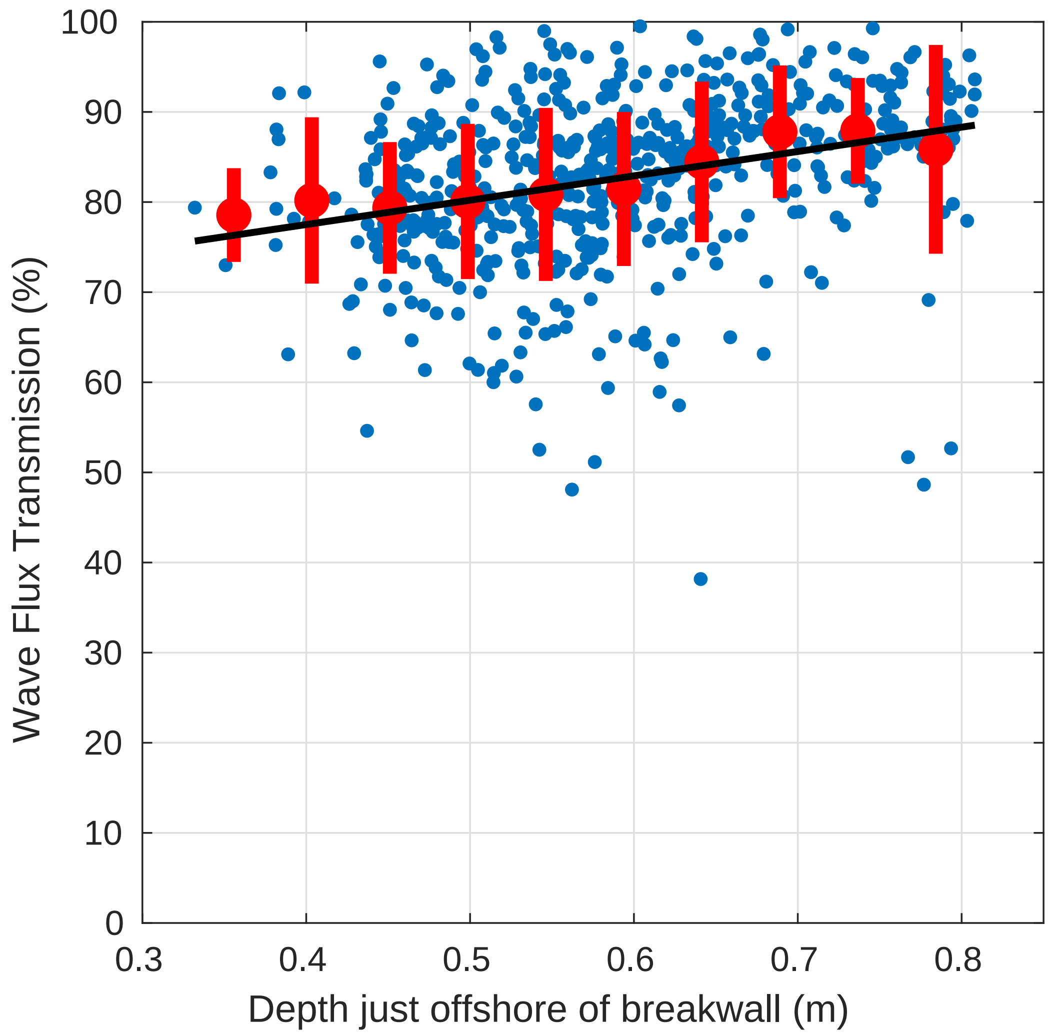

Figure 10: Rates of wave energy flux transmission from NP site N2 (just offshore of the breakwall) to N3 (just onshore of the breakwall) as a function of depth. Blue dots are the estimates from the wake events; the big red dots are averages over 5-cm-wide depth bins; vertical red bars show ± standard deviation; the black curve is a least squares fit through the estimates. Note the higher number of wake events at NP (673) compared to GTM (290) and its contribution to the greater visual spread of data points here compared to Figure 9.

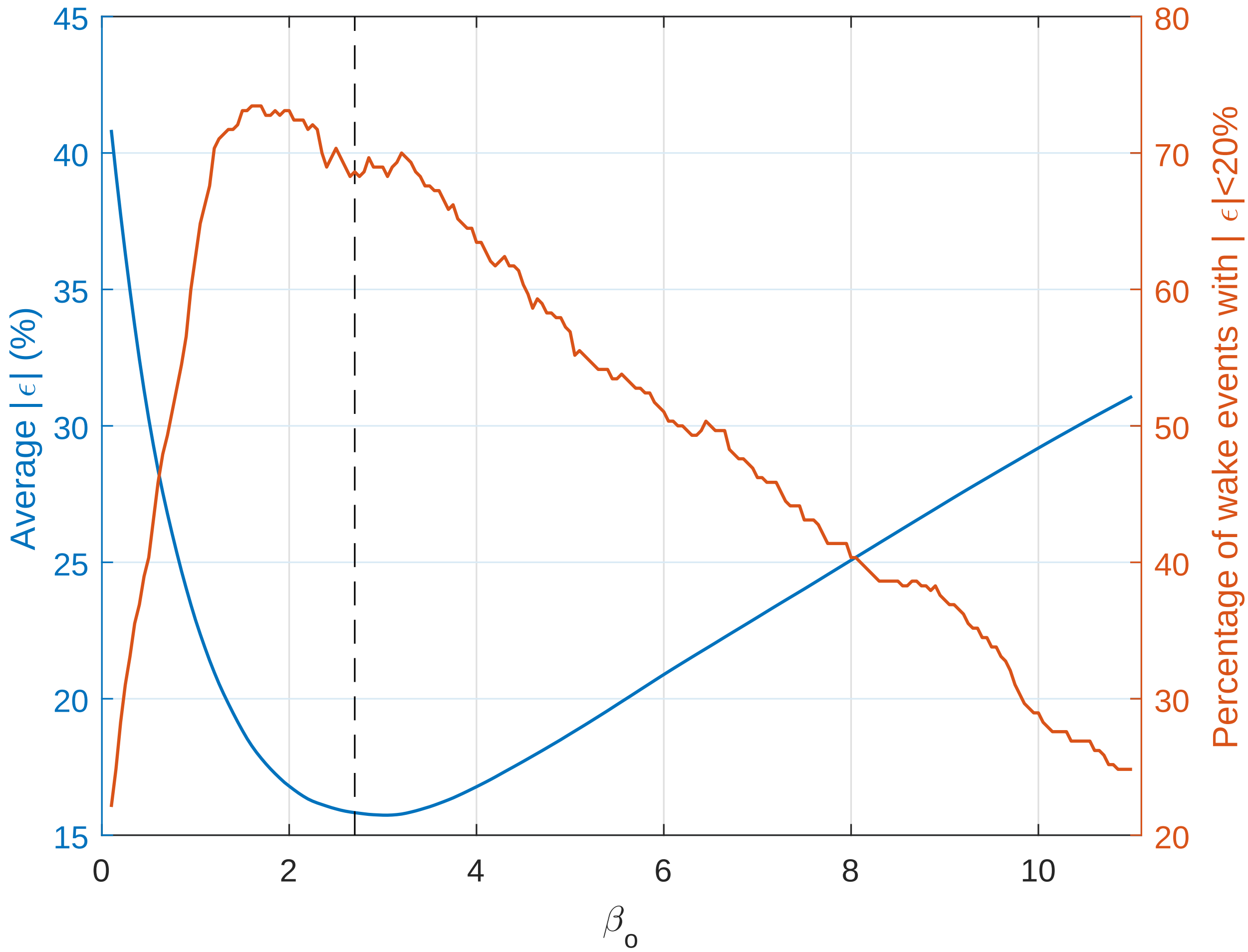

Figure 11: Variations of absolute relative discrepancy between wave transmission estimates based on observations and theoretical estimates ($|\varepsilon|$) averaged over all 290 wake events at GTM (left panel; blue curve) and percentage of wake events with $|\varepsilon|$ less than 20% (right panel; red curve) as a function of turbulent friction coefficient (β_o). Black dashed line indicates the optimum β_o=2.7 that was found to minimize the $\overline{|\varepsilon|}$.

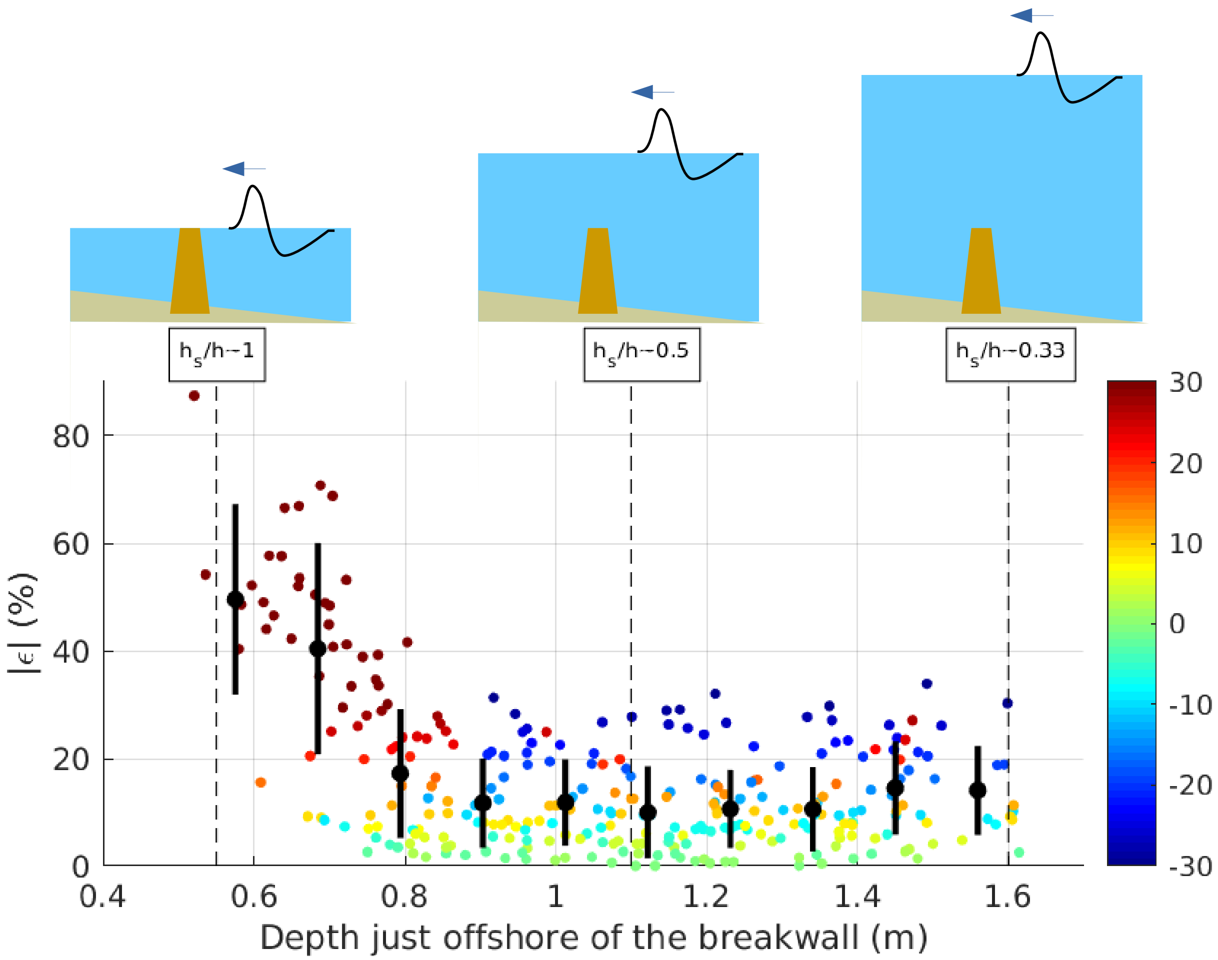

Figure 12: Relative discrepancy (%) between wave transmission estimates based on the observations at GTM and theoretical estimates as a function of water depth. The color coding indicates the sign of discrepancy such that warm colors (positive values) correspond to overestimation by theory and cool colors (negative values) correspond to underestimation by theory (Equation 13). The big black dots are averages over 10-cm-wide depth bins; vertical black bars show $\pm$ standard deviation. Dashed straight lines indicate the conditions the height of the breakwall relative to water depth is equal to 1, 0.5, and 0.33; i.e., h_s/h~1, h_s/h~0.5, and h_s/h~0.33. The sketches at the top panels correspond to these three different conditions of relative breakwall height.

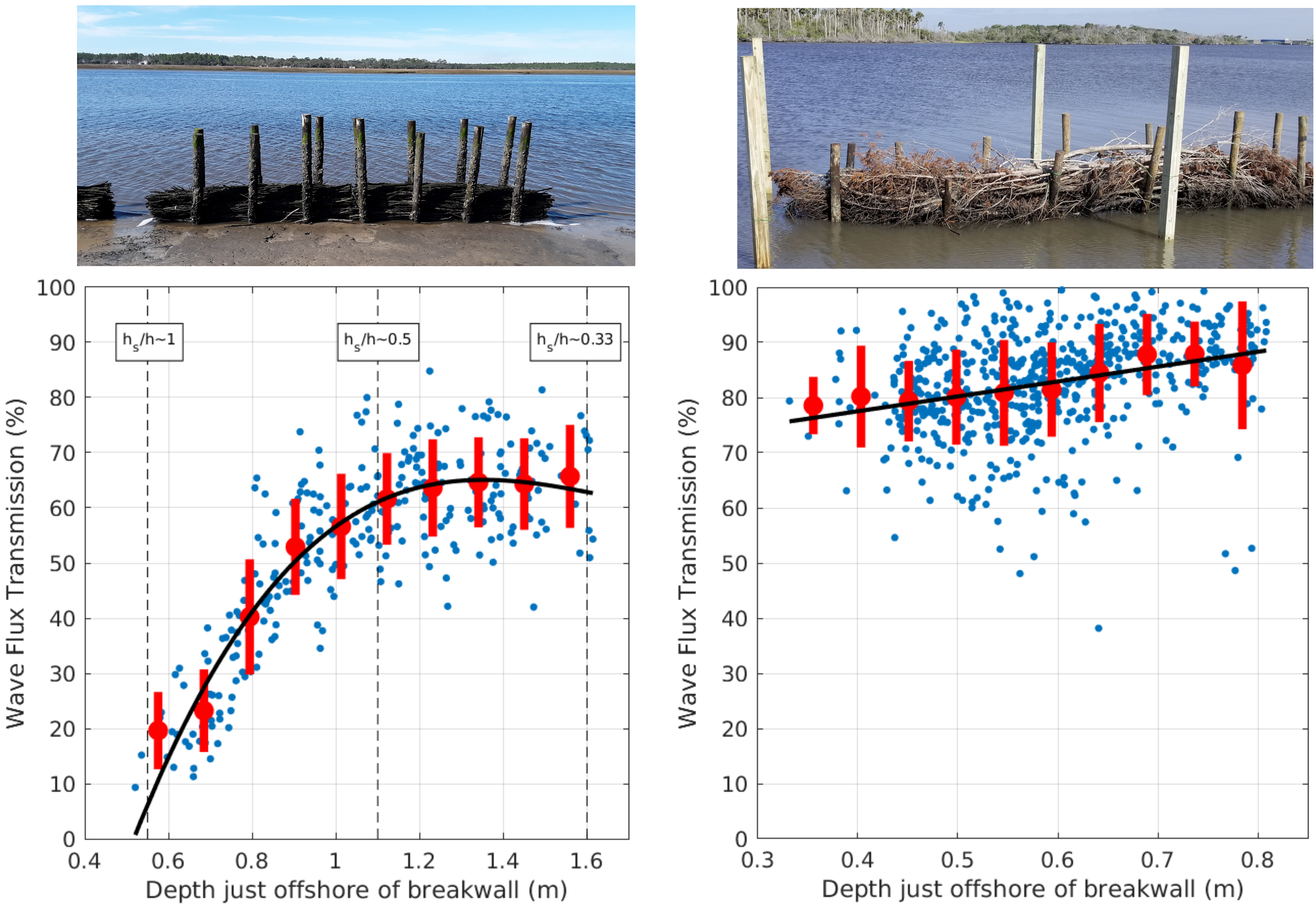
Wave Flux Transmission (%)
Depth just offshore of breakwall (m)
h_s/h~1
h_s/h~0.5
h_s/h~0.33
0
10
20
30
40
50
60
70
80
90
100
0.4
0.6
0.8
1
1.2
1.4
1.6
Wave Flux Transmission (%)
Depth just offshore of breakwall (m)
0
10
20
30
40
50
60
70
80
90
100
0.3
0.4
0.5
0.6
0.7
0.8